

## Supplementary Information

# **Agri-waste derived electroactive Carbon-Iron Oxide nanocomposite for Oxygen Reduction Reaction: An experimental and Theoretical study**

*Pallavi B. Jagdale,<sup>a</sup> Sai Rashmi Manippady,<sup>\*a,b</sup> Rohit Anand,<sup>c</sup> Geunsik Lee,<sup>c</sup> Akshaya Kumar Samal,<sup>a</sup> Ziyauddin Khan,<sup>d</sup> Manav Saxena<sup>\*a</sup>*

*Corresponding authors:*

*<sup>a</sup> Centre for Nano and Material Sciences, Jain (Deemed-to-be University), Bengaluru, Karnataka-560082, India.*

*<sup>b</sup> Faculty of Chemistry, University of Warsaw, Pasteura 1, 02-093 Warsaw, Poland.*

*<sup>c</sup> Center for Superfunctional Materials, Department of Chemistry, Ulsan National Institute of Science and Technology (UNIST), 50 UNIST-gil, Ulsan, 44919 South Korea.*

*<sup>d</sup> Laboratory of Organic Electronics Department of Science and Technology, Linköping University Norrköping, SE-60174 Sweden.*

Email: manavsaxena19@gmail.com; s.manav@jainuniversity.ac.in (MS)

| <b>S. No.</b> | <b>Table of contents</b>                                                                                                                                                                            |
|---------------|-----------------------------------------------------------------------------------------------------------------------------------------------------------------------------------------------------|
| Table S1      | Comparative literature study                                                                                                                                                                        |
| Figure S1     | (a,c,e,g) N <sub>2</sub> adsorption-desorption isotherm and (b,d,f,h) pore size distribution curves of CFe-0, CFe-1, CFe-2 and CFe-3                                                                |
| Figure S2     | LSV of Fe <sub>3</sub> O <sub>4</sub>                                                                                                                                                               |
| Figure S3     | The side and top view of the optimized pristine Fe <sub>3</sub> O <sub>4</sub> /doped graphite structure.                                                                                           |
| Figure S4     | (a) Three different possible O <sub>2</sub> adsorption sites S <sub>1</sub> , S <sub>2</sub> , and S <sub>3</sub> . (b) The most stable O <sub>2</sub> adsorbed structure (on S <sub>2</sub> site). |
| Figure S5     | EDS of CFe-2                                                                                                                                                                                        |
| Table S2      | Quantification of iron using ICP analysis for CFe-2; Elemental analysis of CFe-0, CFe-1, CFe-2, and CFe-3.                                                                                          |

**Table S1.** Comparative ORR performance with recent literature reports.

| Active material                                | Onset potential (V) | $n_e$   | Current density*<br>(mA/cm <sup>2</sup> ) | Tafel slope (mV/dec) | Stability test                                      | Electrolyte             | Reference |
|------------------------------------------------|---------------------|---------|-------------------------------------------|----------------------|-----------------------------------------------------|-------------------------|-----------|
| Fe/N-C                                         | 0.81                | 3.98    | -5.4                                      | 65.1                 | 5 h                                                 | 50 mM PBS               | 1         |
| S, N co-doped rGO                              | 0.85                | 3.8     | -3.1                                      | -                    | 10,000 cycles                                       | 0.1 M KOH               | 2         |
| N/S-doped CNC/SnO <sub>2</sub>                 | 0.68                | 3.9     | -1.0                                      | -                    | 4 h                                                 | 0.1 M KOH               | 3         |
| CeO <sub>2</sub> /biochar carbon               | 0.79                | 3.9     | -4.4                                      | 96                   | 5000 cycles                                         | 0.1 M KOH               | 4         |
| Nitrogen-functionalized reduced graphene oxide | 0.82                | 4.1     | -3.7                                      | 62                   | -                                                   | 0.1 M KOH               | 5         |
| Fe Phthalocyanine@ Mesoporous Carbon Nitride   | 0.62                | 0.87    | -1.2                                      |                      | Shift in onset potential by 20 mV after 3000 cycles | 0.1 M HClO <sub>4</sub> | 6         |
| Biomass carbon from pine needles               | 0.96                | 3.7-3.9 | -4.8                                      | 62.6                 | 1 h                                                 | 0.1 M KOH               | 7         |
| TAPX-NDI-COF                                   | -                   | ~3.5    | -5.2                                      | 84.2-76.4            | 3 h                                                 | 0.1 M NaOH              | 8         |
| Fe-BN-C catalysts derived from ZIF-8           | 0.96                | 3.5-3.7 | -6.1                                      | -                    | 10 h                                                | 0.1 M KOH               | 9         |
| Fe-N-C-2                                       | 0.96                | ~3.9    | -5.8                                      | 74.9                 | 11 h                                                | 0.1 M KOH               | 10        |
| Fe <sub>3</sub> O <sub>4</sub> @FeNC           | 1.0                 | 3.96    | -6.9                                      | 58.8                 | 11 h                                                | 0.1 M KOH               | 11        |
| FeS/Fe <sub>3</sub> C@NS-C-900                 | -                   | 3.7-4.2 | -6.8                                      | 94                   | 5.6 h                                               | 0.1 M KOH               | 12        |

|                                                                |      |               |      |       |      |                        |                         |
|----------------------------------------------------------------|------|---------------|------|-------|------|------------------------|-------------------------|
| Pt/C                                                           | 0.97 | 3.70-<br>3.86 | -5.7 | 106.6 | 11 h | 50 mM Fe <sub>28</sub> | 13                      |
| Fe <sub>3</sub> O <sub>4</sub> partially graphitized composite | 0.82 | 3.76-<br>3.94 | -7.7 | 86    | 40 h | 0.1 M KOH              | <b>Present<br/>work</b> |

**Figure S1:** (a,c,e,g)  $N_2$  adsorption-desorption isotherm and (b,d,f,h) pore size distribution curves of CFe-0, CFe-1, CFe-2 and CFe-3.

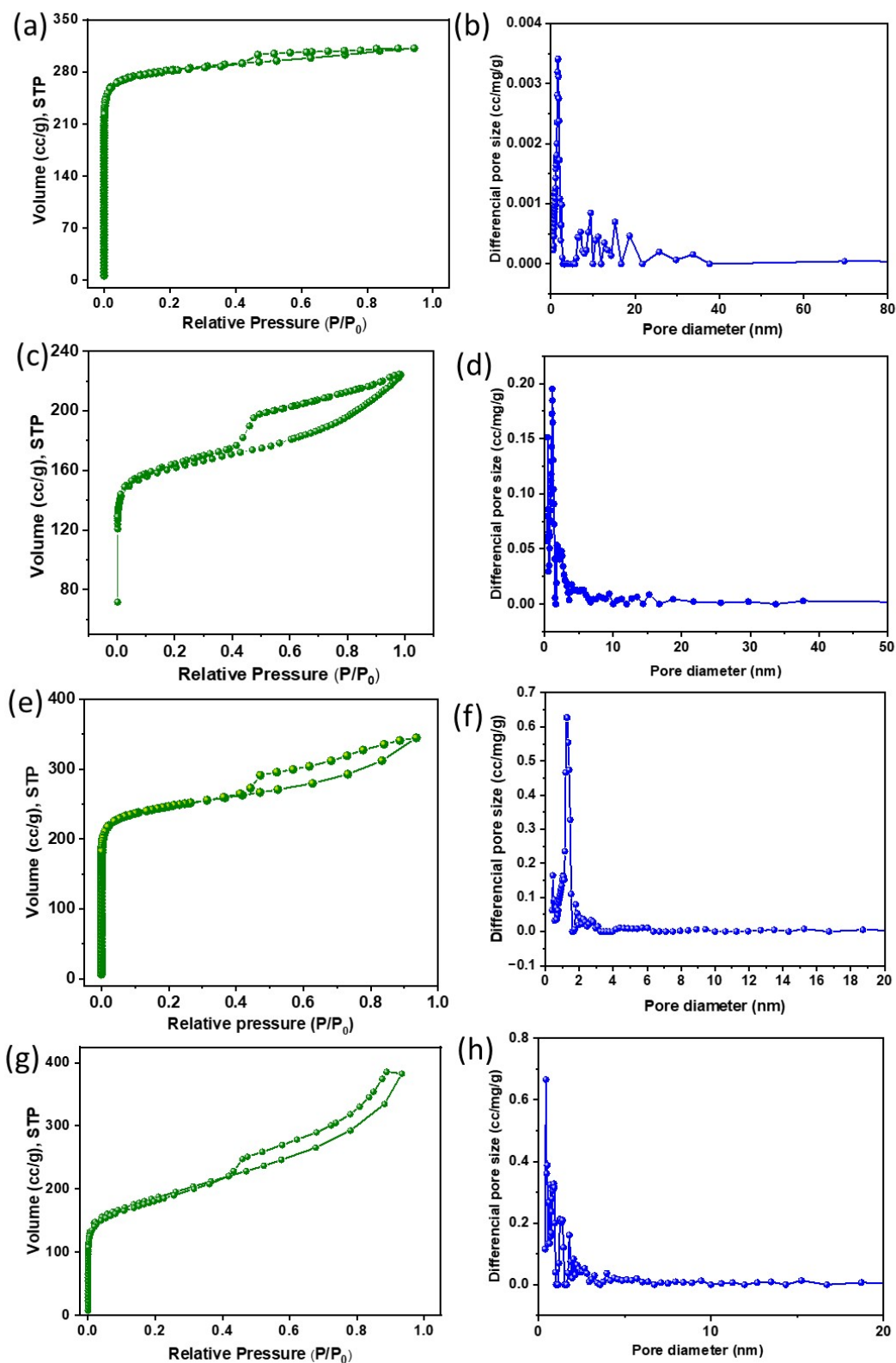
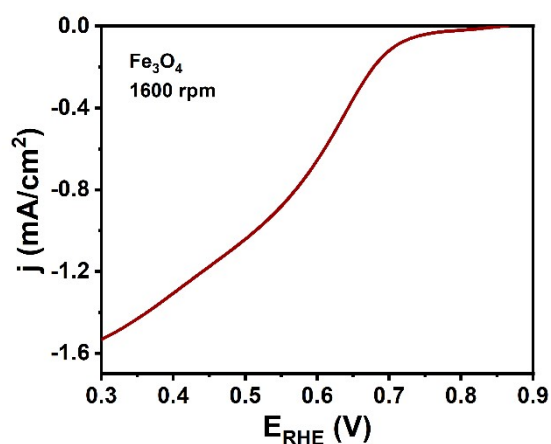


**Figure S2.** LSV of Fe<sub>3</sub>O<sub>4</sub> at 1600 rpm



**Theoretical study:**

**Figure S3** shows the side and top view of the pristine CFe-2 structure. The interlayer distance between the Fe<sub>3</sub>O<sub>4</sub> (022 plane) and graphite in the optimized heterostructure is 3.29 Å, whereas the interlayer distance for graphene sheets is 3.7 Å. Firstly, we considered possible adsorption sites of oxygen molecule on the surface. As illustrated in **Figure S4**, three different favorable binding sites for oxygen are identified: one on the top of tetragonal Fe (S1), the second (S2) and third (S3) are on the edge of differently bonded surface Fe. Compared to other sites, S2 exhibits the lowest adsorption energy, indicating that it is the most thermodynamically stable. In the charge density difference (CDD) figure the yellow-colored electron cloud around adsorbed O atom indicates the accumulation of charge, while the cyan colored electron cloud around active Fe illustrates the loss of electrons.

**Figure S3.** The side and top view of the optimized pristine CFe-2 structure.

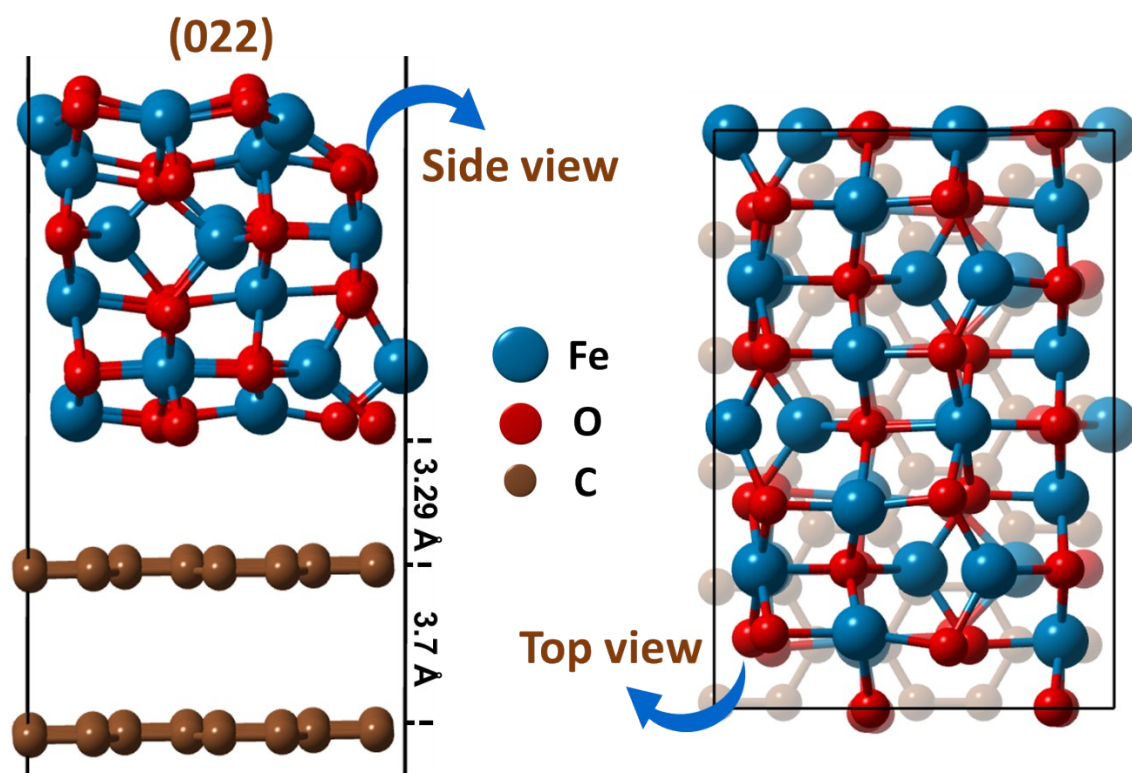


**Figure S4. (a)** Three different possible O<sub>2</sub> adsorption sites S<sub>1</sub>, S<sub>2</sub>, and S<sub>3</sub>. **(b)** The most stable O<sub>2</sub> adsorbed structure (on S<sub>2</sub> site).

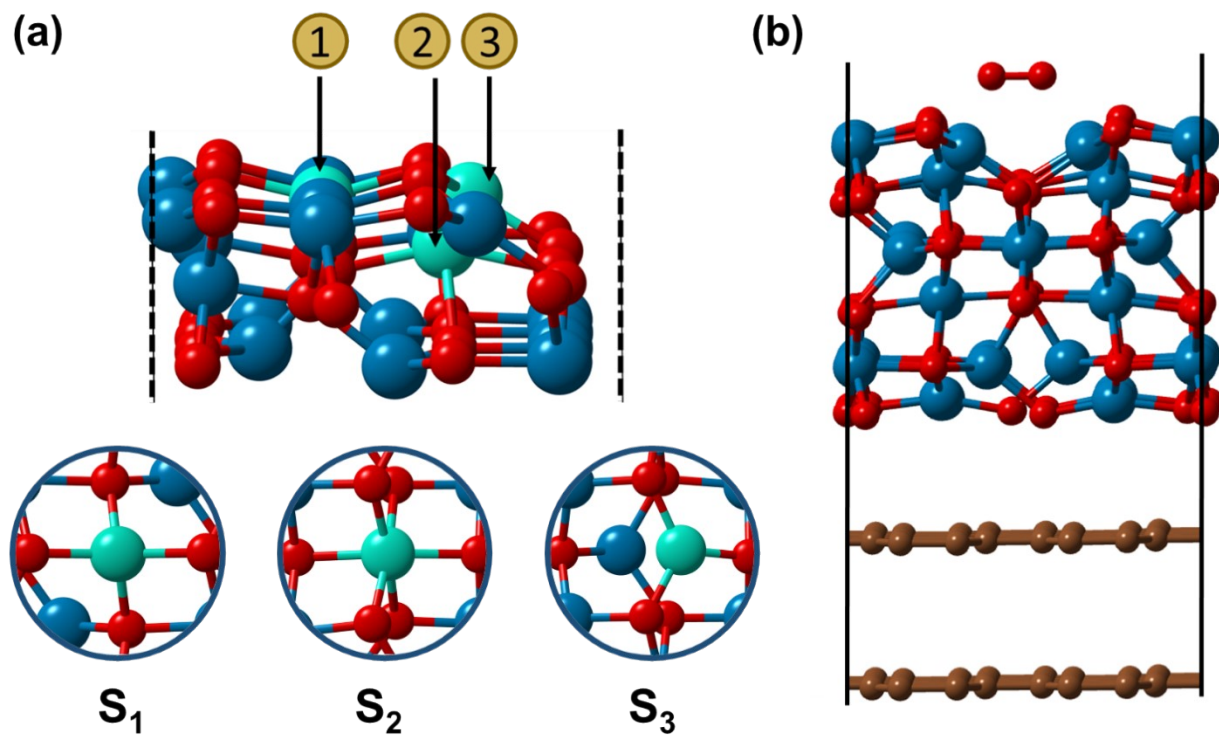


**Figure S5:** EDS of CFe-2.

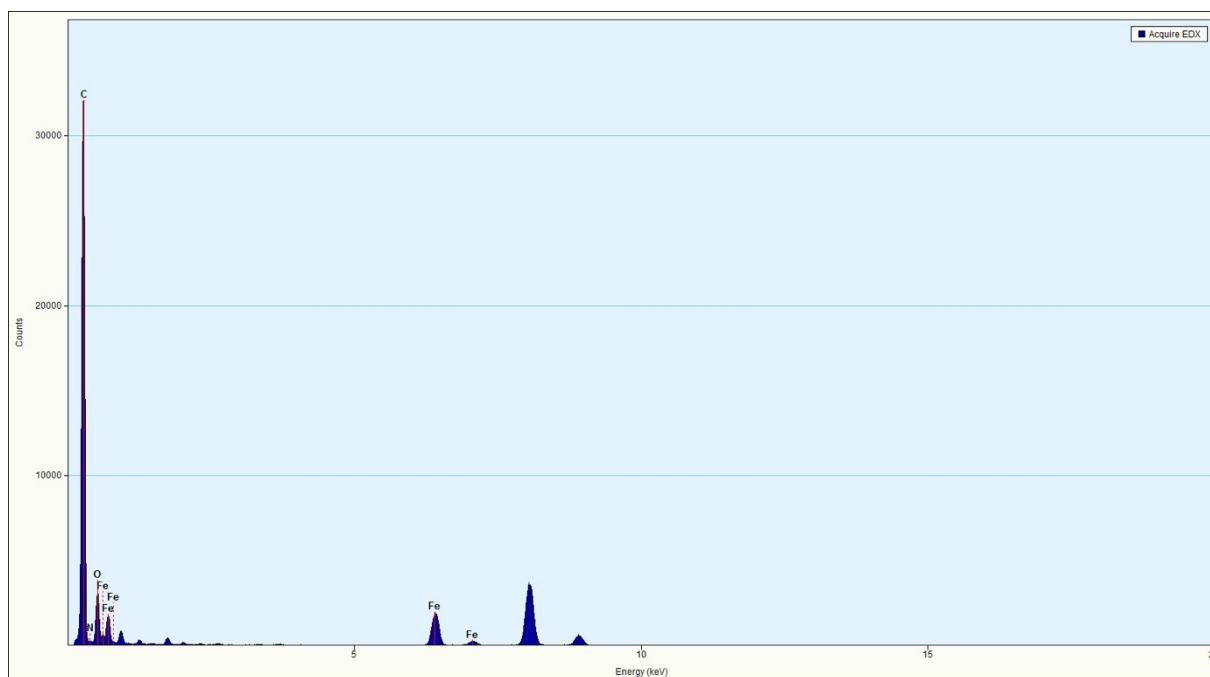




**Table S2.** EDS, XPS, and CHN analysis.

| <b>EDS element quantification (at. %)</b> |          |          |          |                |
|-------------------------------------------|----------|----------|----------|----------------|
|                                           | C (K)    | N (K)    | O (K)    | Fe (K)         |
| <b>CFe-2</b>                              | 93.89    | 0.42     | 4.36     | 1.31           |
| <b>XPS quantification (at. %)</b>         |          |          |          |                |
|                                           | C 1s     | N 1s     | O 1s     | Fe 2p          |
| <b>CFe-2</b>                              | 92.34    | 0.67     | 5.17     | 1.82           |
| <b>CHN analysis</b>                       |          |          |          |                |
| <b>Sample</b>                             | <b>C</b> | <b>H</b> | <b>N</b> | <b>others*</b> |
| <b>CFe-0</b>                              | 52.677   | 2.127    | 1.707    | 43.489         |
| <b>CFe-1</b>                              | 72.001   | 0.862    | 1.834    | 25.303         |
| <b>CFe-2</b>                              | 70.809   | 1.300    | 1.810    | 26.081         |
| <b>CFe-3</b>                              | 61.926   | 0.580    | 1.712    | 35.782         |

\* Contain oxygen and iron content in CFe-1, CFe-2, and CFe-3 and only oxygen for CFe-0.

## References:

1. Z. Fan, J. Li, W. Yang, Q. Fu, K. Sun, Y.-C. Song, Z. Wei, Q. Liao and X. Zhu, *Chem. Eng. J.*, 2020, **385**, 123393.
2. G. Periyasamy, K. Annamalai, I. Patil and B. Kakade, *Diamond and Related Materials*, 2021, **114**, 108338.
3. G. Gianola, N. Garino, M. Bartoli, A. Sacco, C. Pirri and J. Zeng, *Materials Chemistry and Physics*, 2023, **308**, 128205.
4. N. Bhuvanendran, S. Ravichandran, S. Kandasamy, W. Zhang, Q. Xu, L. Khotseng, T. Maiyalagan and H. Su, *International Journal of Hydrogen Energy*, 2021, **46**, 2128-2142.
5. D. Roy, S. Sarkar, K. Bhattacharjee, K. Panigrahi, B. K. Das, K. Sardar, S. Sarkar and K. K. Chattopadhyay, *Carbon*, 2020, **166**, 361-373.
6. D. K. Singh, V. Ganesan, D. K. Yadav and M. Yadav, *Langmuir*, 2020, **36**, 12202-12212.
7. J. Gao, X. Chu, C. He, Z. Yin, H. Lu, J. Feng and X. Tan, *Journal of Applied Electrochemistry*, 2020, **50**, 1257-1267.
8. M. Martínez-Fernández, E. Martínez-Periñán, S. Royuela, J. I. Martínez, F. Zamora, E. Lorenzo and J. L. Segura, *Applied Materials Today*, 2022, **26**, 101384.
9. J. Ma, W. Zhang, F. Yang, Y. Zhang, X. Xu, G. Liu, H. Xu, G. Liu, Z. Wang and S. Pei, *RSC Advances*, 2024, **14**, 4607-4613.
10. J. Li, M. Lin, W. Huang, X. Liao, Y. Ma, L. Zhou, L. Mai and J. Lu, *Small Methods*, 2023, **7**, 2201664.
11. L. Li, Y. Li, Y. Xiao, R. Zeng, X. Tang, W. Yang, J. Huang, K. Yuan and Y. Chen, *Chemical Communications*, 2019, DOI: 10.1039/C9CC03153G.
12. Y.-W. Li, W.-J. Zhang, J. Li, H.-Y. Ma, H.-M. Du, D.-C. Li, S.-N. Wang, J.-S. Zhao, J.-M. Dou and L. Xu, *ACS Applied Materials & Interfaces*, 2020, **12**, 44710-44719.
13. J. Q. Lv, Z. L. Lang, J. Q. Fu, Q. Lan, R. Liu, H. Y. Zang, Y. G. Li, D. D. Ye and C. Streb, *Angew. Chem., Int. Ed. Engl.*, 2022, e202202650.